To cite this article: LIANG X, CHEN J T, WANG R L, et al. The uncertainty quantification of ship shock environment subjected to non-contact underwater explosion[J/OL]. Chinese Journal of Ship Research, 2020, 15(6). http://www.ship-research.com/EN/Y2020/V15/I6/128.

DOI: 10.19693/j.issn.1673-3185.01826

The uncertainty quantification of ship shock environment subjected to non-contact underwater explosion

LIANG Xiao[1], *CHEN Jiangtao*[2], *WANG Ruili*[*3], *HU Xingzhi*[2]

1 School of Mathematics, Shandong University of Science and Technology, Qingdao 266590, China

2 China Aerodynamics Research and Development Centre, Mianyang 621000, China

3 Institute of Applied Physics and Computational Mathematics, Beijing 100094, China

Abstract: [**Objectives**] To identify and quantify uncertain factors in the modeling and simulation of ships suffering a non-contact underwater explosion, the influence of high dimensional random variables on the output of the system is studied. [**Methods**] Following statistical characteristics and engineering knowledge, the normal distribution log is used to describe uncertain physical quantity, and Beta distribution is utilized to depict uncertain empirical parameters. Rosenblatt transformation is explored to transform these correlated random variables into Gaussian variables, satisfying identical and independent distribution. There are a variety of uncertain factors due to the complexity of the model. The computational efficiency is greatly improved when homogeneous Wiener chaos with quadratic adaptive basis function is used to tackle improbability propagation of these input uncertainties. Concerns over a spring device in the deck, expectation, standard deviation, confidence interval, and the probability density function of the quantity of impulsive is presented via the proposed method. [**Results**] Oscillation of the ship always exists after the arrival of a shock wave. The oscillation of the standard deviation is much more forceful than the mean value. [**Conclusions**] The result can be used to predict the impact of a detonation and provide guidance for the reinforcement ability of the ship.

Key words: adaptive basis function; uncertainty quantification; non-contact underwater explosion; unitary transformation; Rosenblatt transformation; homogeneous Wiener chaos

CLC number: U674.7^{+}02

0 Introduction

Non-contact underwater explosions of ships are complex nonlinear multi-physical processes, which still cannot be understood in a full-system full-spatiotemporal scale [1-4]. Three methods are mainly used in studying underwater explosions: experimentation, theoretical calculation, and numerical simulation [1, 3, 5-6]. After World War II, western sea powers conducted underwater explosion tests with real ships[7-8] to directly observe explosion damage, evaluate the shock resistance of the ships and judge the feasibility of installing candidate equipment on ships. However, such real-ship-based tests have inherent defects, such as high costs, uncontrollable processes, and damage to the marine ecological environment. In contrast, numerical simulation is safe, environmentally friendly, low-cost, and process-

Received: 2019 − 11 − 16 **Accepted**: 2020 − 02 − 26

Supported by: National Numerical Wind tunnel Project (NNW2019ZT7-A13); Natural Science Foundation of Shandong Province (ZR2017BA014); Special Topics on Scientific Challenges (TZ2018001)

Authors: Liang Xiao, male, born in 1984, Ph.D., associate professor. Research interest: uncertainty quantification of detonation systems. E-mail: mathlx@163.com

Chen Jiangtao, male, born in 1984, Ph.D., associate researcher. Research interests: aircraft design and computational aerodynamics. E-mail: chenjiangtao@163.com

Wang Ruili, male, born in 1964, Ph.D., researcher, doctoral supervisor. Research interest: development of computational fluid dynamics software. E-mail: wang_ruili@iapcm.ac.cn

Hu Xingzhi, male, born in 1989, Ph.D., associate researcher. Research interests: uncertainty quantification and optimization in spacecraft design. E-mail: huxingzhi99@163.com

***Corresponding author**: WANG Ruili

controllable. However, modeling and simulation (M&S) involves many uncertainties, and thus its predictive ability is doubted by decision-makers.

Combining the advantages of both experimental and numerical methods, uncertainty quantification (UQ) can improve the credibility and reliability of numerical models. In recent years, UQ, as a new discipline, has attracted special attention from European and American scholars, and widely used in major engineering fields such as nuclear energy[9-11], safety [12-13], and aerospace [14-18]. Underwater explosion tests with real ships started late in China, thus resulting in limited available samples. Moreover, foreign public data available for reference are also scarce. As a result, research on UQ methods of ships subjected to non-contact underwater explosions in China has a broad application prospect. However, research on the UQ of ships subjected to non-contact underwater explosions has not been reported so far. This is partially because M&S of underwater explosions is complex and special, which makes it impossible to directly use existing mature methods.

Firstly, the M&S of underwater explosions involves many uncertainties of different types. Specifically, the process contains un-eliminable uncertainties caused by inherent fluctuation of physical quantities and technical errors in measurements. Besides, considering the need for data fitting, it uses uncertainties with no physical significance and empirical parameters that cannot be experimentally calibrated. Secondly, the prerequisite for common UQ methods at present is that random variables obey the independent identical distribution (IID). However, random variables of underwater explosions are not fully obedient to IID. Thirdly, some uncertain physical quantities are required to be strictly non-negative. This makes the common Gaussian distribution in probability statistics infeasible for direct use. For example, on the assumption that mass is normally distributed, non-physical cases with samples of negative mass will occur theoretically. Finally, if parameters are assumed to be uniformly distributed, the boundedness of the parameters can be easily satisfied. However, the high discontinuity of probability density functions (PDFs) of uniform distribution makes it difficult to transform this distribution into a normal distribution. Therefore, the selection of a reasonable probability distribution that accords with statistical results is crucial for studying the UQ of ships subjected to non-contact underwater explosions.

As to UQ methods, Monte Carlo (MC) method is popular. However, it has slow convergence. An effective alternative to the MC method is the polynomial chaos (PC) method, which is also a common method for large-scale engineering calculation[19-23]. The involvement of many uncertainties in M&S of ships subjected to non-contact underwater explosion makes the multivariate PC method easily trapped in a "curse of dimensionality". In short, when the classical method with five quadrature points is used to calculate an underwater explosion system driven by 11-dimensional random variables, it is necessary to run the program $5^{11}\approx4.9\times10^{7}$ times. Moreover, the quintic polynomial needs to be expanded (PC truncation length [24]) (11+5)!/(11! 5!)−1=4 367 times. This requires the program to be run about 5×10^{11} times totally, which exceeds the current computing power. By contrast, the method of homogeneous Wiener chaos based on adaptive basis functions improves the PC method and can alleviate the "curse of dimensionality". In this method, new random basis functions are obtained through the isomorphic unitary transformation of random basis functions. Thus, probabilities of physical quantities to be measured under the expansion of the new random basis functions are concentrated in a low-dimensional subspace.

In view of this, this paper focused on using homogeneous Wiener chaos based on adaptive basis functions to deal with ships subjected to non-contact underwater explosions with high-dimensional uncertainty. First, we gave statistical information such as expectations, standard deviations, and confidence intervals of system outputs by designing a simple test device. Then, we analyzed, quantified, and evaluated the effects of uncertainties on ship shock environments under non-contact underwater explosions. Relevant results can improve the reliability, credibility, and predictive ability of the mathematical model, providing a basis for ship structural design and on-board equipment installation.

1 Mathematical-physical model

The pressure of underwater explosions is related to time and positions and cannot be easily measured. Therefore, the following empirical formula is required for pressure determination[1-2, 25].

$$p(r,t)=p_{\mathrm{m}}(r)f\left(\frac{t}{\theta(r)}\right) \tag{1}$$

where p_m is peak pressure; t is time; r is slope distance; $\theta(r)$ is an attenuation constant. According to Cole's formula [1], there are

$$p_m = K_1\left(\frac{\sqrt[3]{W}}{r}\right)^{\alpha} \tag{2}$$

$$\theta(r) = K_2\left(\frac{\sqrt[3]{W}}{r}\right)^{\beta}\sqrt[3]{W} \tag{3}$$

$$f(x) = a\exp(-a_1 x) + b\exp(-b_1 x) \tag{4}$$

where W is mass of TNT; $f(x)$ is an empirical function; a, b, a_1, b_1, K_1, K_2, α, and β are all empirical parameters, whose values are to be determined.

Shock resistance of ship-borne equipment for the US Navy is a basis of ship structural design and onboard equipment installation. As shown in Fig. 1, an incident wave is decomposed into two parts at a ship-water interface (fluid-structure interaction boundary). One is a refracted wave that penetrates the deck, and the other is a reflected wave that is reflected back into the water. Net pressure after reflection is a result of the algebraic operation of the incident and reflected waves.

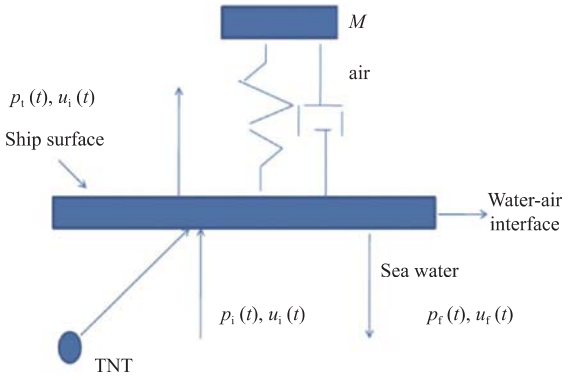

Fig. 1 Force analysis of experimental setup

In the figure, $p_i(t)$ and $u_i(t)$ are the pressure and displacement caused by an incident wave, respectively; $p_f(t)$ and $u_f(t)$ are the pressure and displacement caused by a reflected wave, respectively; $p_t(t)$ is the pressure caused by a transmitted wave; $x(t)$ is the displacement in the outer normal direction of the deck, and m is the areal density of the deck. Due to the great size of the hull, the mass of the spring-system test device is ignored in calculating areal density. According to Newton's laws of motion, in the outer normal direction of the deck, we have

$$m\frac{\mathrm{d}^2x}{\mathrm{d}t^2} = p_t(t) \tag{5}$$

$$p_t(t) = p_i(t) - p_f(t) \tag{6}$$

$$\frac{\mathrm{d}x}{\mathrm{d}t} = \frac{\mathrm{d}u_i}{\mathrm{d}t} - \frac{\mathrm{d}u_f}{\mathrm{d}t} \tag{7}$$

According to the wave-front compatibility relationship [1, 25], there are

$$p_i(t) = \rho c\frac{\mathrm{d}u_i}{\mathrm{d}t} \tag{8}$$

$$p_f(t) = \rho c\frac{\mathrm{d}u_f}{\mathrm{d}t} \tag{9}$$

where ρ is the density of sea water, with ρ =1 027 kg/m^3; c is the local speed of sound, with c =1 493 m/s. $p_i(t)$ is determined by Formula (1).

As shown in Fig. 1, the spring-system test device on the deck produces simple harmonic vibration under the action of the transmitted wave. It is assumed that $y(t)$ is the absolute displacement of the test device in the outer normal direction, and $z(t) = y(t) - x(t)$ is the relative displacement of the test device in the outer normal direction. According to Newton's second law, there is

$$M\frac{\mathrm{d}^2z}{\mathrm{d}t^2} + \mu\frac{\mathrm{d}z}{\mathrm{d}t} + kz = -p_i(t) \tag{10}$$

where M is the mass of the test device, with the spring mass being ignored; μ is a stiffness coefficient of spring; k is a damping coefficient. According to Formulas (5)−(10), we have

$$\frac{\mathrm{d}^2z}{\mathrm{d}t^2} + 2\beta\frac{\mathrm{d}z}{\mathrm{d}t} + \omega^2 z = -\frac{m}{M}\frac{\mathrm{d}^2x}{\mathrm{d}t^2} \tag{11}$$

In the formula,

$$2\beta = \frac{\mu}{M}, \omega^2 = \frac{k}{M}$$

where ω is the natural frequency of the spring system.

2 Uncertainty mining, quantification, and propagation

2.1 Uncertainty sources and quantification

Many uncertainties exist in the interaction between a non-contact underwater explosion and a ship, which can be divided into two categories: One refers to uncertain physical quantities, and the other refers to uncertain empirical parameters (also known as "fitted coefficients"). In Table 1, ξ_1−ξ_6 are uncertain physical quantities that can be calibrated experimentally. In Table 2, ξ_7−ξ_{14} are uncertain empirical parameters that cannot be calibrated experimentally.

It is assumed that the uncertain physical quantities ξ_1−ξ_6 able to be calibrated experimentally obey lognormal distribution. This assumption is made based on statistical results of physical quantities. In addition, lognormal distribution can strictly guarantee non-negativity of physical quantities, and parameters of the lognormal distribution LN [τ, σ] can be determined just by expectations and standard devia-

tions of low orders (where τ is a logarithmic expectation and σ is a logarithmic standard deviation). Formula (12) gives calculation formulas of τ and σ.

$$\tau = \lg\left(\frac{E(\boldsymbol{\xi})^2}{\sqrt{std(\boldsymbol{\xi})^2 + E(\boldsymbol{\xi})^2}}\right)$$
$$\sigma = \sqrt{\lg\left(\frac{E^2(\boldsymbol{\xi}) + std(\boldsymbol{\xi})^2}{E(\boldsymbol{\xi})^2}\right)} \quad (12)$$

where $E(\xi)$ is the expectation of the random variable ξ; $std(\xi)$ is the standard deviation of ξ.

The explosion of a torpedo was taken as an example. Due to the action of waves and undercurrents, this kind of weapon is difficult to stay in a fixed position. Moreover, it explodes in motion, which makes position determination more difficult. As a result, the physical quantity ξ_1 representing the slope distance r is uncertain. It is supposed that ξ_1 satisfies $E(\xi_1)$ = 10 m and $std(\xi_1)$ =0.2 m. Then, from Formula (12), we have μ_{ξ_1}=2.032, σ_{ξ_1}=0.02. Spherical TNT explosives used in this paper will fluctuate randomly due to voids and gaps during processing and mix with impurity particles. This can result in uneven coagulation of particles, thus making density distribution [9,10,19] of the explosives random.

In addition, the physical quantity ξ_2 representing the mass W of TNT satisfies $E(\xi_2)$ =100 kg and $std(\xi_2)$ =2 kg. By calculation based on Formula (12), we have μ_{ξ_2}=4.605, σ_{ξ_2}=0.120. For the physical quantities ξ_3 representing the areal density m of the deck and ξ_4 representing the mass M of the test device, their measured values fluctuate due to uncertainties in measurement. Their statistical characteristics satisfy $E(\xi_3)$ =80 kg, $std(\xi_3)$ =6 kg, $E(\xi_4)$ = 1 800 kg, and $std(\xi_4)$ =200 kg. By calculation based on Formula (12), we have μ_{ξ_3}=4.379, σ_{ξ_3}=0.078 9, μ_{ξ_4}=7.489 4, σ_{ξ_4}=0.111, respectively. The randomness of the physical quantities ξ_5 representing the stiffness coefficient and ξ_6 representing the damping coefficient is caused by inherent properties of materials. Statistical characteristics of these quantities satisfy $E(\xi_5)$ = 1.8 × 10^7 N/m, $std(\xi_5)$ =1.8×10^5 N/m, $E(\xi_6)$ =52 000 Ns/m, and $std(\xi_6)$ = 200 Ns/m, respectively. By calculation based on Formula (12), we have μ_{ξ_5}=16.705, σ_{ξ_5}=0.010, μ_{ξ_6}=10.859, σ_{ξ_6}= 0.004.

As mentioned above, empirical parameters cannot be calibrated experimentally. They are generally defined within a certain range according to engineering experience and assumed to be of a Beta probability distribution. Although uniform distribution can also limit value ranges of parameters, it is difficult to transform uniform distribution into a normal distribution, due to the high discontinuity of the density function. This is why the Beta probability distribution is applied in this paper. Specifically, the parameters χ and β in the Beta probability distribution [χ, β, a, b] determine the curve shape of the PDF. The parameters a and b give upper and lower limits of random variables, and they are determined based on the experience of engineers [1,3,7]. Fig. 2 shows PDF images of random variables (uncertain physical quantities) to directly describe statistical characteristics of uncertainties.

Table 1 Uncertainty of a ship subjected to a non-contact underwater explosion (physical quantities)

Symbol	Uncertain physical quantity	Lognormal probability distribution
ξ_1	Slope distance r/m	[2.302, 0.020]
ξ_2	TNT mass W/kg	[4.605, 0.120]
ξ_3	Areal density of deck m/(kg·m^{-2})	[4.379, 0.078 9]
ξ_4	Mass of test device M/kg	[7.489 4, 0.111]
ξ_5	Stiffness coefficient of spring μ/(N·mm)	[16.705, 0.010]
ξ_6	Damping coefficient k/(Ns·m^{-1})	[10.859, 0.004]

Table 2 Uncertainty of a ship subjected to a non-contact underwater explosion (empirical parameters)

Symbol	Uncertain empirical parameter	Beta probability distribution
ξ_7	a	[2, 2, 0.82, 0.83];0.83]
ξ_8	b	[2, 2, 0.16, 0.18]
ξ_9	a_1	[3, 4, 1.2, 1.4]
ξ_{10}	a_2	[3, 4, 0.175, 0.185]
ξ_{11}	K_1	[5, 4, 50, 54]
ξ_{12}	K_2	[5, 4, 0.88, 0.94]
ξ_{13}	α	[3, 4, 1.12, 1.14]
ξ_{14}	β	[3, 4, −0.20, −0.16]

2.2 Rosenblatt transformation

The premise of homogeneous Wiener chaos with quadratic adaptive basis functions is that random variables must be standard normal ones satisfying IID. However, from Section 2.1, this condition is not met. In this paper, Rosenblatt transformation [26] is used to transform correlated random variables into a group of independent random variables obeying standard normal distribution. The specific steps are as follows: $\{X_1, X_2, \ldots, X_n\}$ is supposed to be a list of random variables (where the subscript n re-

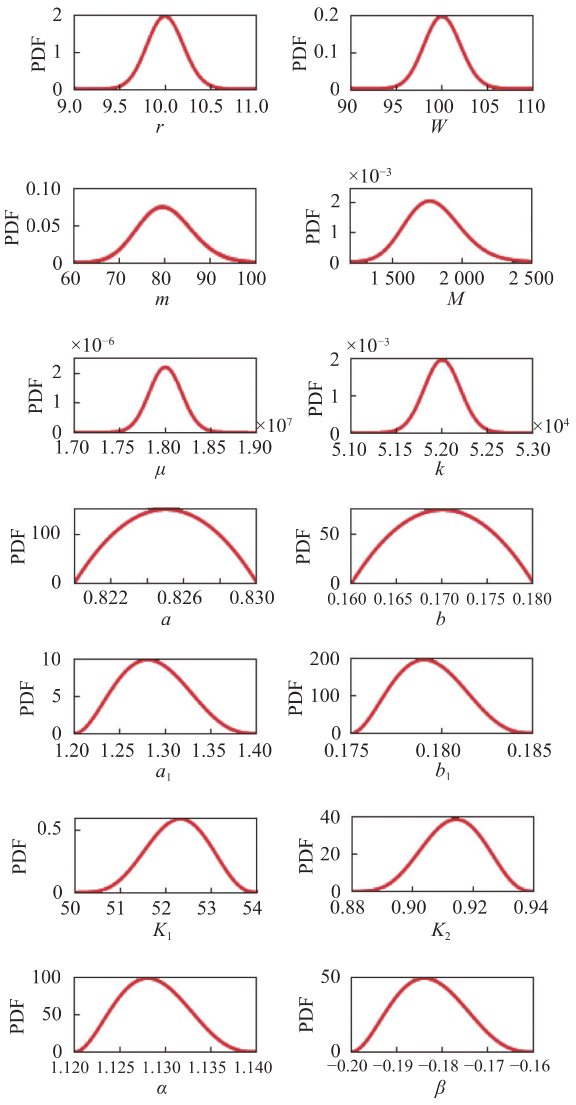

Fig. 2 PDF of random variables

fers to the number of random variables). Let

$$F_{Y_n}(y_n|y_1,y_2,\cdots,y_{n-1}) = F_{X_n}(x_n|x_1,x_2,\cdots,x_{n-1})$$

where

$$F_{Y_n}(y_n|y_1,y_2,\cdots,y_{n-1}) = P\{Y_n \leqslant y_n|Y_1=y_1,Y_2=y_2,\cdots,Y_{n-1}=y_{n-1}\}$$

represents conditional probability. Thus,

$$y_n = F_{Y_n}^{-1}(F_{X_n}(x_n|x_1,x_2,\cdots,x_{n-1})|y_1,y_2,\cdots,y_{n-1})$$

Then, $\{Y_1, Y_2, \ldots, Y_n\}$ obeys standard normal distribution and is independent of each other.

2.3 Wiener chaos with quadratic adaptive basis functions

We set Ω as a sample space, $\mathcal{F}$ as a σ-algebra in Ω, P: $\mathcal{F}\rightarrow[0, 1]$ as a probability measure defined in $\mathcal{F}$, the Gelfand triple $(\Omega, \mathcal{F}, P)$ as a complete probability space, and $L^2(\Omega)$ as a square-integrable space in Ω.

Given an inner product $<fg>=\int_\Omega f(\theta)g(\theta)\mathrm{d}P(\theta)$, with $f, g \in L^2(\Omega)$ (where θ is an integral element in the sense of Lebesgue; $f, g \in L^2(\Omega)$ is a generalized function), a Hilbert space can be formed.

Suppose that $\{\xi_i\}_{i=1}^d$ indicates all random variables in Tables 1 and 2 (the superscript d refers to dimension). After Rosenblatt transformation, it can be transformed into a group of standard independent Gaussian random variables. Displacement of the spring system satisfies Formulas (1) − (11), where $\boldsymbol{\xi} = [\xi_1, \xi_2, \ldots, \xi_d]^{\mathrm{T}}$. From Tables 1 and 2, we have d =14.

According to the Cameron-Martin theorem[21-23, 27], there is

$$z(t,\boldsymbol{\xi}) = \sum_{\alpha\in\mathcal{I}} z_\alpha(t)\Psi_\alpha(\boldsymbol{\xi}) \tag{13}$$

where $\alpha = (\alpha_1, \alpha_2, \ldots, \alpha_d)$ is a character set (Lebesue space); $\mathcal{I} = \mathbf{N}^d$, ($\mathbf{N}$ is a set of natural numbers); $z_\alpha(t) \triangleq < z(t,\boldsymbol{\xi})\Psi_\alpha(\boldsymbol{\xi}) >$ ($z_\alpha(t)$ is an expansion coefficient), and

$$\begin{aligned}\Psi_\alpha &= \frac{H_\alpha(\boldsymbol{\xi})}{\sqrt{\alpha!}}\\ H_\alpha(\boldsymbol{\xi}) &= \prod_{i=1}^{d} h_{\alpha_i}(\xi_i)\\ \boldsymbol{\alpha}! &= \prod_{i=1}^{d}\alpha_i!\\ \|H_\alpha(\boldsymbol{\xi})\|_{L^2(\Omega)} &= \boldsymbol{\alpha}!\end{aligned} \tag{14}$$

In the above formulas, $h_{\alpha_i}(\xi_i)$ is a univariate Hermite polynomial of the α_i^{th} order; $H_\alpha(\boldsymbol{\xi})$ is a multivariate Hermite polynomial.

H=*Span*$\{\xi_1, \xi_2, \ldots, \xi_d\}$ is defined. $H^{:n:}$ is assumed to be the space generated by d-dimensional n^{th}-order random Hermite polynomials. According to the Wiener-Ito-Segal isomorphism formula [28], we have $L^2(\Omega) = \oplus_n H^{:n:}$. In practical application, Formula (13) needs to be truncated by limited times, namely,

$$z^p(t,\boldsymbol{\xi}) \triangleq \sum_{\alpha\in\mathcal{I}_p} z_\alpha(t)\Psi_\alpha(\boldsymbol{\xi}) \tag{15}$$

where $p \triangleq (n+d)!/(n!d!)-1$, is the number of expansions of an n^{th}-order polynomial; $\mathcal{I}_p = \{|\boldsymbol{\alpha}| \leqslant p | |\boldsymbol{\alpha}| = \alpha_1+\alpha_2+\cdots+\alpha_d\}$, and in the sense of mean square, there is $\lim_{p\to\infty} z^p(t, \boldsymbol{\xi}) = z(t, \boldsymbol{\xi})$.

2.3.1 Basis transformation

$\boldsymbol{A}$ represents a unitary matrix in $\boldsymbol{R}^d$ (where $\boldsymbol{R}$ is the Euclidian space). We define

$$\boldsymbol{\eta} = \boldsymbol{A}\boldsymbol{\xi} \tag{16}$$

where $\boldsymbol{\eta}$ is a linear transformation of uncertainties $\boldsymbol{\xi}$ of underwater explosions, which is also a group of bases of H mathematically, and $H^{:n:}$ can also be generated by $\boldsymbol{\eta}$. The displacement of the spring system is expressed as follows:

$$z^A(t,\boldsymbol{\eta}) \triangleq z(t,\boldsymbol{\xi}),\ \Psi_\alpha^A(\boldsymbol{\xi}) = \Psi_\alpha(\boldsymbol{\eta}) \tag{17}$$

namely,

$$z(t,\boldsymbol{\xi})=\sum_{\alpha\in\mathcal{I}_p}z_\alpha(t)\Psi_\alpha(\boldsymbol{\xi})=\sum_{\beta\in\mathcal{I}_p}z_\beta(t)\Psi_\beta(\boldsymbol{\xi}) \quad (18)$$

Therefore,

$$z_\beta^A(t)=\sum_{\alpha\in\mathcal{I}_p}z_\alpha(t)<\Psi_\alpha\Psi_\beta^A>=\sum_{\alpha,|\alpha|=|\beta|}z_\alpha(t)<\Psi_\alpha\Psi_\beta^A> \quad (19)$$

2.3.2 Model simplification based on the projection method

$V_I=\mathcal{L}(\Psi_\beta)$, $\boldsymbol{\beta}\in\mathcal{I}$ and $\mathcal{I}\subset\mathcal{I}_p$ are set. Then, the projection of displacement of the spring device onto V_I is defined as follows:

$$z^{A,\mathcal{I}}(t,\boldsymbol{\xi})=z^{\mathcal{I}}(t,\boldsymbol{\eta})=\sum_{\beta\in\mathcal{I}}\sum_{\alpha\in\mathcal{I}_p}z_\alpha(t)\Psi_\beta(\boldsymbol{\eta})<\Psi_\alpha\Psi_\beta^A> \quad (20)$$

In addition, the projection of $z^{A,\mathcal{I}}(t,\boldsymbol{\eta})$ onto V_I can be expressed as

$$z^{A,\mathcal{I}}(t,\boldsymbol{\eta})=\sum_{\gamma\in\mathcal{I}}z_\gamma^{\mathcal{I}}(t)\Psi_\gamma(\boldsymbol{\xi}) \quad (21)$$

Therefore,

$$z_\gamma^{\mathcal{I}}(t)=\sum_{\beta\in\mathcal{I}}\sum_{\alpha\in\mathcal{I}_p}z_\alpha(t)<\Psi_\alpha\Psi_\beta^A><\Psi_\beta\Psi_\gamma> \quad (22)$$

Then, limiting z to V_I yields $z_\gamma^{\mathcal{I}}=\{z_\gamma,\boldsymbol{\gamma}\in\mathcal{I}\}$.

2.3.3 Solving coefficients of Wiener chaos based on quadratic adaptive basis functions by non-intrusive method

$\boldsymbol{A}$ and $\mathcal{I}$ are selected by the quadratic adaptive method. Let

$$z=z_0+\sum_{i=1}^d\hat{z}_i\xi_i+\sum_{i=1}^d\sum_{j=1}^d\hat{z}_{ij}(\xi_i\xi_j-\delta_{ij})+\sum_{|\alpha|\geqslant3}z_\alpha(t)\Psi_\alpha(\boldsymbol{\xi}) \quad (23)$$

where z_0 is the expectation of displacement z; $\hat{z}_i=z_{\boldsymbol{e}_i}$, $\hat{z}_{\boldsymbol{e}_{ij}}=z_{ij}/\sqrt{2}$, among them, $\boldsymbol{e}_i$ is a subset of I_p, and it is a unit vector in which the i^{th} element is not 1 and the other elements are all zero; ξ_i and ξ_j are random variables in Tables 1 and 2, respectively; δ_{ij} is the Kronecker's delta. The main part of Formula (23) can be rewritten as

$$z_{II}=z_0-\sum_{i=1}^d z_{ii}+\sum_{i=1}^d\hat{z}_i\xi_i+\sum_{i=1}^d\sum_{j=1}^d\hat{z}_{ij}\xi_i\xi_j \quad (24)$$

Where $\hat{z}_{ii}=z_{2\boldsymbol{e}_i}/\sqrt{2}$. Let

$$\boldsymbol{S}=\frac{1}{\sqrt{2}}\begin{pmatrix}z_{2\boldsymbol{e}_1}&z_{\boldsymbol{e}_1+\boldsymbol{e}_2}&\cdots&z_{\boldsymbol{e}_1+\boldsymbol{e}_d}\\z_{\boldsymbol{e}_2+\boldsymbol{e}_1}&z_{2\boldsymbol{e}_2}&\cdots&z_{\boldsymbol{e}_2+\boldsymbol{e}_n}\\\vdots&\vdots&\vdots&\vdots\\z_{\boldsymbol{e}_n+\boldsymbol{e}_1}&z_{\boldsymbol{e}_n+\boldsymbol{e}_2}&\cdots&z_{2\boldsymbol{e}_n}\end{pmatrix} \quad (25)$$

According to Formula (23), there is

$$\boldsymbol{A}\boldsymbol{S}\boldsymbol{A}^{\mathrm{T}}=\boldsymbol{D} \quad (26)$$

where $\boldsymbol{D}$=diag{d_1, d_2, ..., d_d}. According to linear algebra, $\boldsymbol{A}$ and $\boldsymbol{D}$ are the eigenvector and eigenvalue matrix of $\boldsymbol{S}$, respectively. Specifically, $\boldsymbol{A}$ is a unitary matrix. Then, we have

$$z^A(\boldsymbol{\eta})=z_0+\sum_{i=1}^d b_i\eta_i+\sum_{i=1}^d d_i(\eta_i^2-1)+\sum_{|\boldsymbol{\beta}|\geqslant3}z_\beta(t)\Psi_\beta(\boldsymbol{\eta}) \quad (27)$$

where $b_i=\sum_{j=1}^d a_{ij}z_{\boldsymbol{e}_j}$. Let

$$\mathcal{I}\triangleq\mathcal{E}=\bigcup_{i=1}^d\mathcal{E}_i$$

Then,

$$z^{A,\mathcal{I}}(\boldsymbol{\eta})=z_0+\sum_{i=1}^d\sum_{\beta\in\boldsymbol{e}_i}z_\beta^A(t)\Psi_\beta(\boldsymbol{\eta}) \quad (28)$$

The error between $z^A(\boldsymbol{\eta})$ and $z^{A,\mathcal{I}}(\boldsymbol{\eta})$ is as follows:

$$z^A(\boldsymbol{\eta})-z^{A,\mathcal{I}}(\boldsymbol{\eta})=\sum_{p\geqslant|\boldsymbol{\beta}|\geqslant3}z_\beta^A(t)\Psi_\beta(\boldsymbol{\eta}) \quad (29)$$

The coefficients of Formula (24) are solved by the non-intrusive method, namely,

$$z_\beta^A\approx\sum_{r=1}^s z^{A,\mathcal{I}}(t,\boldsymbol{\eta}^{(r)})\Psi_\beta(\boldsymbol{\eta}^{(r)})w_r,\ \boldsymbol{\beta}\in\varepsilon \quad (30)$$

where $\boldsymbol{\eta}^{(r)}$ and w_r are quadrature points and weights, respectively. Specifically, $\boldsymbol{\eta}^{(r)}=\eta_1{}^{(r)},\eta_2{}^{(r)},\cdots,\eta_d{}^{(r)}$; s is the number of quadrature points; $z^{A,\mathcal{I}}(t,\boldsymbol{\eta}^{(r)})$ satisfies Formulas (1)−(11), and $\boldsymbol{\xi}^{(r)}=\boldsymbol{A}^{-1}\boldsymbol{\eta}^{(r)}$.

3 Analysis of UQ results

With the method described in Section 2, in the case of p=2, Formula (24) is equivalent to Formula (31).

$$z^{A,\mathcal{I}}(\boldsymbol{\eta})=z_0+\sum_{i=1}^d z_i^A\eta_i+\sum_{i=1}^d z_{ii}^A\frac{(\eta_i^2-1)}{\sqrt{2}}$$
$$z_i^A=\sum_{j=1}^d a_{ij}z_{\boldsymbol{e}_j},\ z_{ii}^A=\sqrt{2}d_i \quad (31)$$

Figs. 3−6 show the expectation, standard deviation, and confidence interval of relative displacement $z(t)$ of the test device in the outer normal direction, calculated according to the method in Section 2.

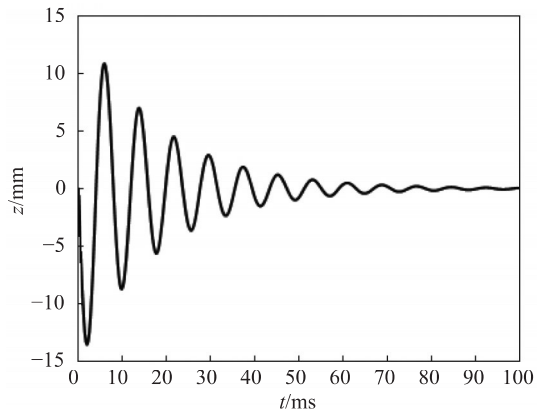

Fig. 3 Expectation for displacement z in the spring system

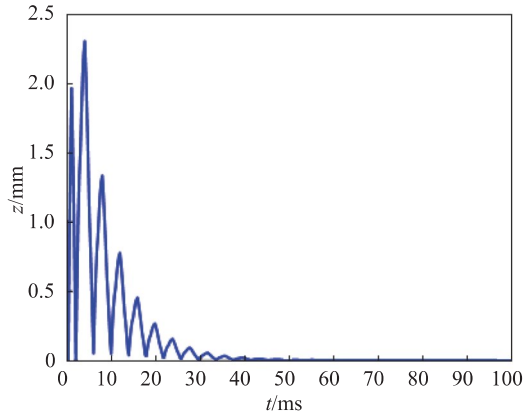

Fig. 4 Standard deviation for displacement z in the spring system

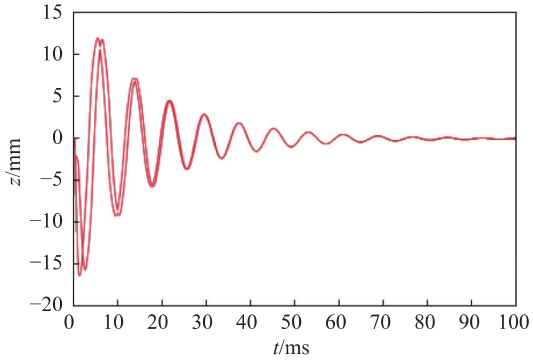

Fig. 5 Confidence interval for displacement z in the spring system

As can be seen from Fig. 3, after 100 ms, the expectation of $z(t)$ gradually approaches zero, with slight oscillations. This indicates that the deck remains in an oscillatory state after being subjected to underwater explosions.

As can be seen from Fig. 4, the standard deviation of $z(t)$ tends to be zero after 40 ms. This indicates that the effects of underwater explosion shock on the system are mainly concentrated in the initial 100 ms. After 100 ms, the effects of explosion shock waves are negligible. This indicates that the ship oscillates most obviously in the first 10 ms of explosion shock, and resistance against explosion shock at this time is crucial.

$E|z(t)|$ reaches a maximum of 12.3 mm at 1.87 ms, while $std(z(t))$ reaches a maximum of 2.38 mm at 3.86 ms. Therefore, the time for the standard deviation to reach the peak is longer than that for the expectation to do so. This is mainly caused by inertia.

From the comparison between Fig. 3 and Fig. 4, the standard deviation of $z(t)$ oscillates more violently than the expectation does, and the standard-deviation curve is of poor smoothness.

As can be seen from Fig. 5, the confidence interval of $z(t)$ widens quickly within 10 ms and reaches

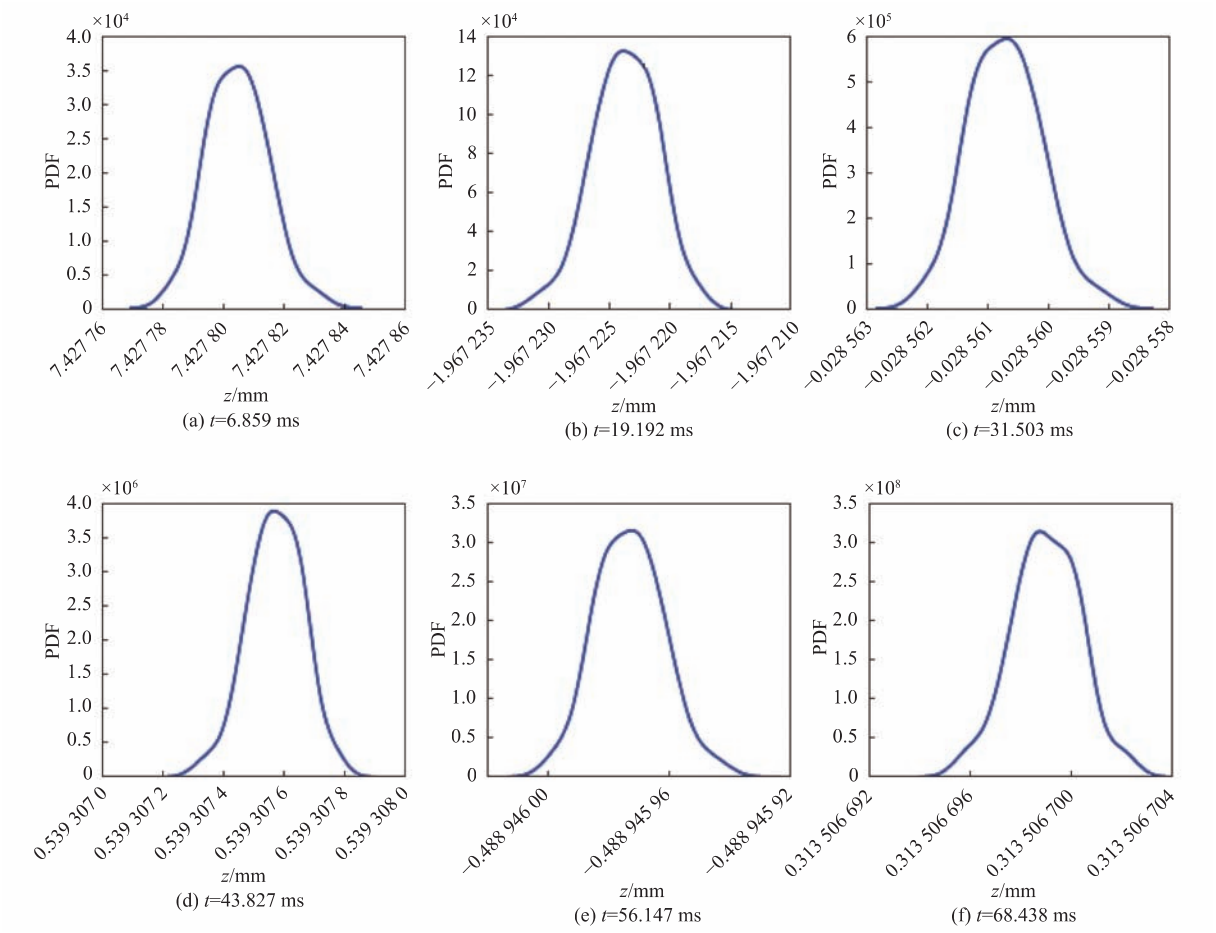

Fig. 6 PDF of displacement z in spring system at different time

a maximum width at 8.65 ms. Then, it gradually narrows and tends to be zero. This indicates that uncertainties are high and difficult to be predicted at the initial time, but it is precisely the most important moment for ship protection. Moreover, from Fig. 5, prediction after 40 ms is accurate. Although the explosion shock wave still oscillates at this time, it gradually disappears.

Fig. 6 shows the PDF curves of $z(t)$ with six selected moments as observation points to obtain more accurate oscillations of equipment on the deck. The PDF curves are roughly bell-shaped, which is consistent with cognition. Moreover, other statistical characteristics of $z(t)$ at these moments can also be obtained according to the above results, such as peaks and skewness.

As can also be seen from Fig. 6, with the passage of time, the variation range of $z(t)$ narrows and the PDF peak increases, while the skewness appears alternately. In conclusion, with the method in this paper, it is easier to predict long-time dynamic behavior than initial dynamic behavior.

4 Conclusions

By designing a suitable spring-system test device, this paper studied the effects of uncertainties in underwater explosions of medium and low intensity on the test device on deck through probability statistics. In addition, it gave expectations, standard deviations, confidence intervals, and PDFs of displacement of the test device by using homogeneous Wiener chaos based on adaptive basis functions. The main conclusions are as follows:

1) The deck subjected to underwater explosion shock remains in an oscillatory state. The expectation and standard deviation of the spring-system test device gradually approach zero after reaching maximum values, and the confidence interval gradually narrows. The oscillation of the standard deviation is much greater than that of the expectation, and the standard deviation lags behind the expectation in reaching the maximum. Therefore, in the case of a ship attacked by non-contact underwater weapons, its damage in the initial stage of explosion shock is the greatest and difficult to be predicted. Thus, ship protection at this time is crucial.

2) Homogeneous Wiener chaos based on adaptive basis functions alleviates the "curse of dimensionality" to some extent. Specifically, it constructs isomorphic unitary transformation of random basis functions, selects an appropriate projection space, and uses the structure of system response in low-dimensional space to approach that in the whole system. Thus, computational efficiency is improved and computational costs are saved. This method is feasible. For example, for the expansion of a quintic polynomial, the truncation length in the case of standard multivariate PC is $(14+5)!/14!5!-1 = 46\,512-1 = 46\,511$, while that in the case of homogeneous Wiener chaos based on adaptive basis functions is $(1+5)!/1!5!-1 = 5$, with an efficiency of $46\,511/5 \approx 10^4$.

The method in this paper can be used to guide ship designers to predict oscillations of objects on deck and judge the damage impact of torpedoes for providing ship personnel with suggestions about protective measures. Besides, it can give ship reinforcement standards and determine the feasibility of on-board equipment installation. Homogeneous Wiener chaos based on adaptive basis functions can also be extended to the study of other impact responses of ships.

In conclusion, UQ research of ships subjected to non-contact underwater explosions is a systematic project, which requires the cooperation of experts in oceanology, engineering, mathematics, and physics. Only preliminary results are given in this paper. The following issues will be considered in future work.

1) This paper lacks a comparison between experimental and numerical results, without obtaining real experimental data yet. Therefore, in the next step, we plan to work with experts in this field to study propagation and quantification of uncertainties in underwater explosion tests and compare experimental results with numerical ones to confirm model parameters.

2) Effects of model uncertainties are not considered in this paper. In fact, with explosives of different types, peak pressure, attenuation constants, and even fitting functions will be different. Even for the same type of explosives, different empirical functions may be employed for representation. Therefore, studying the effects of different empirical functions on system outputs, that is, quantification of model form uncertainties will always be an important topic in UQ research.

Acknowledgements

We would like to thank the Visiting Scholar Program of Shandong University of Science and Technology for its financial support to the first author during his visit to the University of Southern Cali-

fornia. Moreover, we would like to thank Professor Roger Ghanem from the University of Southern California for his suggestions on this topic.

References

[1] COLE R H. Underwater explosion [M]. New Jersey: Princeton University Press, 1948.

[2] GEERS T L, HUNTER K S. An integrated wave-effects model for an underwater explosion bubble [J]. The Journal of the Acoustical Society of America, 2002, 111 (4): 1584−1601.

[3] SHIN Y S. Ship shock modeling and simulation for far-field underwater explosion [J]. Computers & Structures, 2004, 82 (23/24/25/26): 2211−2219.

[4] YAO X L, YE X, ZHANG A M. Cavitation bubble in compressible fluid subjected to traveling wave [J]. Acta Physica Sinica, 2013, 62 (24): 244701 (in Chinese).

[5] XU W Z, WU W G. Development of in-house high-resolution hydrocode for assessment of blast waves and its application [J]. Chinese Journal of Ship Research, 2017, 12 (3): 64−74 (in Chinese).

[6] ZHANG A M, WANG S P, PENG Y X, et al. Research progress in underwater explosion and its damage to ship structures [J]. Chinese Journal of Ship Research, 2019, 14 (3): 1−13 (in Chinese).

[7] DAS S, RHANEM R. Uncertainty analysis in ship shock modeling and simulation [C]//Proceedings of 74th Shock and Vibration Symposium. San Diego, CA: [s.n.], 2003.

[8] SHIN Y S, SANTIAGO L D. Surface ship shock modeling and simulation: two-dimensional analysis [J]. Shock and Vibration, 1998, 5 (2): 129−137.

[9] SLOAN J, SUN Y W, CARRIGAN C. Uncertainty quantification for discrimination of nuclear events as violations of the comprehensive nuclear-test-ban treaty [J].Journal of Environmental Radioactivity, 2016, 155−156: 130−139.

[10] LIANG X, WANG R L. Sensitivity analysis and validation of detonation computational fluid dynamics model [J]. Acta Physica Sinica, 2017, 66 (11): 116401 (in Chinese).

[11] KOZMENKOV Y, KLIEM S, ROHDE U. Validation and verification of the coupled neutron kinetic/thermal hydraulic system code DYN3D/ATHLET [J]. Annals of Nuclear Energy, 2015, 84 (1): 153−165.

[12] LIANG X, WANG R L. Verification and validation of detonation modeling [J]. Defence Technology, 2019, 15 (3): 398−408.

[13] PEDERSON C, BROWN B, MORGAN N. The Sedov blast wave as a radial piston verification test [J]. Journal of Verification, Validation and Uncertainty Quantification, 2016, 1 (3): 031001.

[14] HU X Z, CHEN X Q, LATTARULO V, et al. Multidisciplinary optimization under high-dimensional uncertainty for small satellite system design [J]. AIAA Journal, 2016, 54 (5): 1732−1741.

[15] HU X Z, CHEN X Q, PARKS G T, et al. Review of improved Monte Carlo methods in uncertainty-based design optimization for aerospace vehicles [J]. Progress in Aerospace Sciences, 2016, 86: 20−27.

[16] DENG X G, ZONG W G, ZHANG L P, et al. Verification and validation in computational fluid dynamics [J]. Advances in Mechanics, 2007, 37 (2): 279−288 (in Chinese).

[17] ZHANG H X, ZHA J. The uncertainty and truth-value assessment in the verification and validation of CFD [J]. Acta Aerodynamica Sinica, 2010, 28 (1): 39−45 (in Chinese).

[18] WANG X D, KANG S. Application of polynomial chaos on numerical simulation of stochastic cavity flow [J]. Scientia Sinica Technological, 2010, 53 (10): 2853−2861.

[19] TANG T, ZHOU T. Recent developments in high order numerical methods for uncertainty quantification [J]. Scientia Sinica Mathematica, 2015, 45 (7): 891−928 (in Chinese).

[20] WANG R L, JIANG S. Mathematical methods for uncertainty quantification in nonlinear multi-physics systems and their numerical simulations [J]. Scientia Sinica Mathematica, 2015, 45 (6): 723−738 (in Chinese).

[21] LIANG X, WANG R L. Uncertainty quantification of cylindrical test through Wiener chaos with basis adaptation and projection [J]. Explosion and Shock Waves, 2019, 39 (4): 041408 (in Chinese).

[22] GHANEM R G, SPANOS P D. Stochastic Finite Elements: A Spectral Approach [M]. New York: Springer, 1991.

[23] XIU D B, KARNIADAKIS G E. The Wiener-Askey polynomial chaos for stochastic differential equations [J]. SIAM Journal on Scientific Computing, 2002, 24 (2): 619−644.

[24] LIU Q, WANG R L, LIN Z. Uncertainty quantification Lagrangian computational using non-intrusive polynomial chaos [J]. Chinese Journal of Solid Mechanics, 2013, 33 (Supp 1): 224−233 (in Chinese).

[25] PRICE R S. Similitude equations for explosives fired underwater [R]. Washington DC: Naval Surface Warfare Center, 1979.

[26] ROSENBLATT M. Remarks on a multivariate transformation [J]. The Annals of Mathematical Statistics, 1952, 23 (3): 470−472.

[27] LIANG X, WANG R L, GHANEM R. Uncertainty quantification of detonation through adapted polynomial chaos [J]. International Journal for Uncertainty Quantification, 2020, 4 (1): 83−100.

[28] JANSON S. Gaussian Hilbert spaces [M]. Cambridge: Cambridge University Press, 1997.

非接触水下爆炸下舰船冲击环境的不确定度量化

梁霄[1],陈江涛[2],王瑞利*[3],胡星志[2]
1 山东科技大学 数学学院,山东 青岛 266590
2 中国空气动力研究与发展中心,四川 绵阳 621000
3 北京应用物理与计算数学研究所,北京 100094

摘　要:[**目的**]为挖掘和量化舰船非接触水下爆炸建模与模拟中的不确定性因素,开展高维随机变量对系统输出结果的影响研究。[**方法**]根据变量统计特征和工程经验,使用对数正态分布描述物理量的不确定度,使用Beta分布描述唯象参数的不确定度,并使用Rosenblatt变换将不同类型的相关随机变量组转化为服从独立同分布的正态分布变量组。此外,考虑到模型的复杂性且不确定性因素众多,使用基于二次自适应基函数的齐次Wiener混沌方法处理不确定度的传播,以提高计算效率。以甲板上弹簧系统试验装置为例,应用所提方法研究试验装置的冲击响应量的期望值、标准差、置信区间和概率密度函数。[**结果**]结果显示,舰船遭受水下爆炸冲击后,甲板一直处于振荡状,标准差的振荡相比期望值更大。[**结论**]研究结果可为非接触水下爆炸冲击影响以及评估舰船抗冲击性能提供依据。

关键词:自适应基函数;不确定度量化;非接触水下爆炸;酉变换;Rosenblatt变换;齐次Wiener混沌

[*Continued from page* 37]

短路冲击作用下电力推进装置扭振计算与分析

李增光*[1], 赵辉[1], 周宁[2]
1 中国舰船研究设计中心,上海 201108
2 中国大洋矿产资源研究开发协会,北京 100045

摘　要:[**目的**]对于电力推进装置,推进电机短路故障时的瞬态扭矩激励峰值很大,对推进系统的运行安全影响较大。为此,提出一种短路故障工况下推进装置扭振计算方法。[**方法**]根据船舶推进装置扭振分析理论,建立系统的时域扭振计算模型,给出短路时推进电机瞬态冲击扭矩作用下系统的响应计算方法。基于此,建立某电力推进装置的计算模型,对其扭振固有特性及3极和2极短路故障时的系统扭振响应进行计算与分析。[**结果**]结果表明,系统动态特性对短路冲击扭矩的传递具有重要影响,其中,高于系统第1阶弹性模态频率的扭矩成分在传递至推进器端时的衰减很大,推进器处的动态扭矩以第1阶弹性模态频率成分为主,而在推进电机与传动轴—推进器之间设置高弹性联轴器,能大幅衰减冲击扭矩引起的动态响应;瞬态扭矩响应最大值随着电机转速的增加而增加,交变扭矩可达到数倍平均扭矩,由此引起齿轮传动装置的齿面敲击,且传动部件瞬时扭转应力较大。[**结论**]提出的时间域扭振模型及方法可用于电力推进装置在短路瞬态冲击作用下的响应计算分析,在设计阶段对短路冲击作用下的扭振响应进行校核非常必要,可提高电力推进装置运行的安全性。

关键词:电力推进装置;扭转振动;短路故障;冲击